CARBON CYCLE

Microbial oxidation of lithospheric organic carbon in rapidly eroding tropical mountain soils

Jordon D. Hemingway,[1,2]*† Robert G. Hilton,[3] Niels Hovius,[4,5] Timothy I. Eglinton,[6] Negar Haghipour,[6] Lukas Wacker,[7] Meng-Chiang Chen,[8] Valier V. Galy[1]

Lithospheric organic carbon ("petrogenic"; OC_{petro}) is oxidized during exhumation and subsequent erosion of mountain ranges. This process is a considerable source of carbon dioxide (CO_2) to the atmosphere over geologic time scales, but the mechanisms that govern oxidation rates in mountain landscapes are poorly constrained. We demonstrate that, on average, 67 ± 11% of the OC_{petro} initially present in bedrock exhumed from the tropical, rapidly eroding Central Range of Taiwan is oxidized in soils, leading to CO_2 emissions of 6.1 to 18.6 metric tons of carbon per square kilometer per year. The molecular and isotopic evolution of bulk OC and lipid biomarkers during soil formation reveals that OC_{petro} remineralization is microbially mediated. Rapid oxidation in mountain soils drives CO_2 emission fluxes that increase with erosion rate, thereby counteracting CO_2 drawdown by silicate weathering and biospheric OC burial.

Erosion-induced weathering in collisional mountain belts is a major carbon-cycle regulator over million-year time scales and provides a link between tectonics and climate (*1*, *2*). Atmospheric CO_2 is consumed by the export and burial in marine sediments of biospheric organic carbon (OC_{bio}) and carbonate minerals precipitated after silicate rock weathering (*1*). The CO_2 drawdown flux associated with both processes increases with erosion rate (*3*, *4*), highlighting the importance of steep, erosive orogens in driving CO_2 drawdown. By comparison, CO_2 release during exhumation and erosion has received considerably less attention, despite its potential to partially or fully negate the effects of geological CO_2 consumption (*1*, *5*, *6*). Oxidative weathering of sulfide minerals (coupled with carbonate dissolution) and lithospheric, or "petrogenic," organic carbon (OC_{petro}) contained in exhumed rocks can increase atmospheric CO_2 and decrease O_2 concentrations over geologic time scales (*1*, *7*–*9*). However, the mechanisms that govern oxidation rates and efficiencies in mountain belts are underconstrained (*5*, *8*, *9*).

[1]Department of Marine Chemistry and Geochemistry, Woods Hole Oceanographic Institution (WHOI), 266 Woods Hole Road, Woods Hole, MA 02543, USA. [2]Massachusetts Institute of Technology (MIT)–WHOI Joint Program in Oceanography and Applied Ocean Science and Engineering, 77 Massachusetts Avenue, Cambridge, MA 02139, USA. [3]Department of Geography, Durham University, South Road, Durham DH1 3LE, UK. [4]GFZ German Research Center for Geoscience, Telegrafenberg, Potsdam 14473, Germany. [5]Department of Earth and Environmental Sciences, University of Potsdam, Karl-Liebknechtstraße 24, Golm 14476, Germany. [6]Geological Institute, Department of Earth Sciences, ETH Zürich, Sonneggstraße 5, Zürich 8092, Switzerland. [7]Laboratory of Ion Beam Physics, Department of Physics, ETH Zürich, Otto-Stern-Weg 5, Zürich 8092, Switzerland. [8]Taroko National Park Headquarters, Fu-Su Village, Hualien 972, Taiwan. ***Corresponding author. Email: jordon_hemingway@fas.harvard.edu** †Present address: Department of Earth and Planetary Sciences, Harvard University, 20 Oxford Street, Cambridge, MA 02138, USA.

To better constrain orogenic CO_2 emissions, we assessed the controls on OC_{petro} oxidation and export in the Central Range of Taiwan, one of the fastest-exhuming and -eroding mountain belts on Earth (*10*). Steep relief (*11*), frequent typhoon landfalls (*10*), and high bedrock landslide rates (*11*) lead to long-term erosion rates of 3 to 6 mm $year^{-1}$ across the range (*10*). Although supplemental contributions from deeper in the exhumation path are likely, weathering in such mountain landscapes occurs primarily on hillslopes and in colluvial deposits (*12*, *13*). We therefore assessed OC molecular and isotopic evolution in multiple hillslope soil profiles located in the LiWu and WuLu River basins (fig. S1) and verified these observations at the catchment scale by using LiWu River suspended sediments (*14*). Soils at our study sites are ≤ 1 m thick, including mineral (A and E) and saprolite (C) layers (*15*); experience residence times on the order of centuries (*14*); and overlay bedrock ranging from Mesozoic greenschist and amphibolite at low elevations (Tananao schists) to Cenozoic slate and phyllite near the Lishan fault (Pilushan and Lushan Formations) (*16*). All lithologies are carbonaceous, with bedrock outcrops containing 0.2 to 0.7% OC_{petro} (table S1) (*17*).

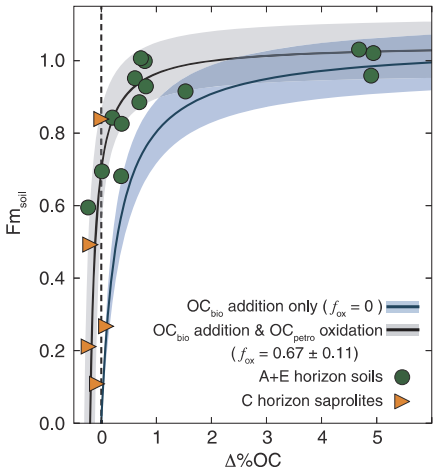

Fig. 1. Evidence for bedrock OC oxidation. The blue line is the solution to Eq. 2, assuming no OC_{petro} oxidation during soil formation (OC_{bio} addition only; f_{ox} = 0). The black line is the orthogonal distance regression best-fit solution that minimizes the residual error between measured (green circles and orange triangles) and predicted Fm_{soil} values. The shaded region around each line is the propagated ±1σ uncertainty (*14*). Best-fit results indicate that 67 ± 11% of bedrock OC is lost during oxidative weathering. Δ%OC = 0 is shown as a vertical dashed line. Measurement error bars (±1σ) are smaller than marker sizes.

We observed substantial OC_{petro} loss in all soil profiles, as evidenced by the relationship between soil OC content ($\%OC_{soil}$) and ^{14}C activity (expressed as "fraction modern" or Fm) (*14*). To account for differences in %OC between bedrock lithologies (*17*), $\%OC_{soil}$ is expressed as

$$\Delta\%OC = \%OC_{soil} - \%OC_{bedrock} \quad (1)$$

where $\%OC_{bedrock}$ is the OC content of bedrock immediately underlying each soil sample. The average fraction of bedrock OC that is oxidized during soil formation, f_{ox}, can then be quantified by utilizing the fact that OC_{petro} is inherently ^{14}C-free (Fm_{petro} = 0.0) and setting Fm_{bio} = 1.045 ± 0.079, the measured ^{14}C activity of vascular plant-wax fatty acids extracted from A- and E-horizon soils (table S2) (*14*). Soil OC is treated as a mixture of OC_{bio} and residual OC_{petro}, leading to the equation (*14*)

$$Fm_{soil} = Fm_{bio}\left[\frac{\Delta\%OC + (f_{ox})(\%OC_{bedrock})}{\Delta\%OC + \%OC_{bedrock}}\right] \quad (2)$$

Fm_{soil} is a hyperbolic function of Δ%OC with curvature that is defined by both $\%OC_{bedrock}$ and f_{ox}, as shown in Fig. 1. We simultaneously solved Eq. 2 for the best-fit $\%OC_{bedrock}$ and f_{ox} values using orthogonal distance regression and accounted for uncertainty using Monte Carlo resampling (*14*).

On average, 67 ± 11% (±1σ) of bedrock OC is lost during soil formation, a minimum estimate because deep weathering has likely already removed OC from the initial bedrock (*18*). To test whether observed %OC trends simply reflect mobile element losses during weathering and not oxidation per se, we solved Eq. 2 for a subset of samples after normalizing OC content to the immobile element titanium (table S1) (*14*). Calculated f_{ox} values using normalized and unnormalized data are identical within uncertainty, indicating no appreciable mobility effect on our results (fig. S2).

Assuming that all OC lost is oxidized to CO_2 (*8*), f_{ox} can be used to estimate the steady-state

CO_2 emission flux from soils owing to OC_{petro} oxidation, termed Φ_{ox}, according to

$$\Phi_{ox} = \frac{(f_{ox})(\%\,OC_{bedrock})(\rho_{soil})(z_{soil})}{\tau_{soil}} \quad (3)$$

where ρ_{soil} is the soil density, z_{soil} is the soil thickness (*15*), and τ_{soil} is the soil residence time on hillslopes. We estimated τ_{soil} using three independent methods (landslide rates, catchment-average denudation rates, and OC_{bio} erosion rates) and incorporated uncertainty for each variable in Eq. 3 using Monte Carlo resampling across the range of observed values (*14*), resulting in a median Φ_{ox} range of 6.1 to 18.6 metric tons C km^{-2} $year^{-1}$ for conditions that are prevalent across the Central Range (fig. S3A) (*14*). We emphasize that Φ_{ox} is a minimum estimate of total CO_2 emissions by OC_{petro} oxidation owing to the potential for OC losses occurring during deep weathering (*18*). Still, this flux is statistically identical to two independent, catchment-integrated OC_{petro} oxidation estimates for Taiwanese rivers—based on fluvial OC_{petro} export (≤12 metric tons C km^{-2} $year^{-1}$) (*19*) and dissolved rhenium yield (7 to 13 metric tons C km^{-2} $year^{-1}$; fig. S3B) (*5*)—and is two to six times as high as estimates of CO_2 drawdown by silicate weathering in the LiWu catchment (fig. S3C) (*18*). The observation that Φ_{ox} matches catchment-integrated emissions implies that OC_{petro} oxidation in Taiwan occurs predominantly in rapidly eroding hillslope soils.

A saprolite depth profile collected from the WuLu catchment indicates that bedrock OC can be oxidized and replaced with OC_{bio} before A and E horizons have fully developed. Two samples collected at 0.5 and 0.2 m depth contain similar OC concentrations (0.20 and 0.28%, respectively) but have drastically different Fm values (0.108 and 0.839, respectively; table S1). Rapid OC_{petro} oxidation can occur (i) abiotically without chemical alteration, (ii) abiotically with chemical alteration, (iii) biotically without chemical alteration, or (iv) biotically with chemical alteration and ^{14}C-depleted biomass production (*20*–*22*). To assess alteration and track multiple OC sources within a single sample, we used Ramped PyrOx (RPO) serial combustion (*23*). This technique heats each sample at a constant ramp rate to separate OC on the basis of thermal lability and determines Fm values for specific temperature intervals (termed RPO fractions) (*14*). To quantitatively compare OC chemical structure, we determined the underlying thermal activation energy (E) distribution for each sample, termed $p(0,E)$, because this is an intrinsic property of carbon bond strength and thus a proxy for chemical composition (*23*). Unlike ^{14}C activity, end-member mixing does not shift OC in E space. Mixing OC_{bio} with unaltered OC_{petro} will thus result in a bimodal $p(0,E)$ distribution, whereas chemical alteration is required to explain the presence of intermediate E values (*14*, *23*).

We constrained bedrock E by using particulate OC (POC) from 27 suspended sediment samples, including isolated ≥2-mm clasts, collected from the LiWu River during four typhoon events (*14*). Because sediment exported during typhoons is dominated by material sourced from bedrock incision, distributed runoff erosion, and landsliding throughout the basin (*11*, *12*), we expect this sample set to integrate outcropped bedrock lithologies that contain relatively unweathered OC_{petro}. This is supported by bulk POC ^{13}C content (expressed as $\delta^{13}C$ values) and total nitrogen to POC ratios (table S3), which span the range of Tananao schist, Lushan Formation, and Pilushan Formation values (*17*). Figure 2A shows that bedrock OC is exclusively associated with $E \geq 185$ kJ mol^{-1} (termed high-E; fig. S3A) (*14*), consistent with the observed partial graphitization of this material (*16*). We additionally constrained vascular-plant OC $p(0,E)$ by using two organic-rich (≥5%) surface soils characterized by bulk Fm values similar to those of plant-wax fatty acids (*14*). For both samples, ≥90% of OC is associated with $E < 150$ kJ mol^{-1} (termed low-E), indicating that OC_{bio} and OC_{petro} are effectively separated in E space.

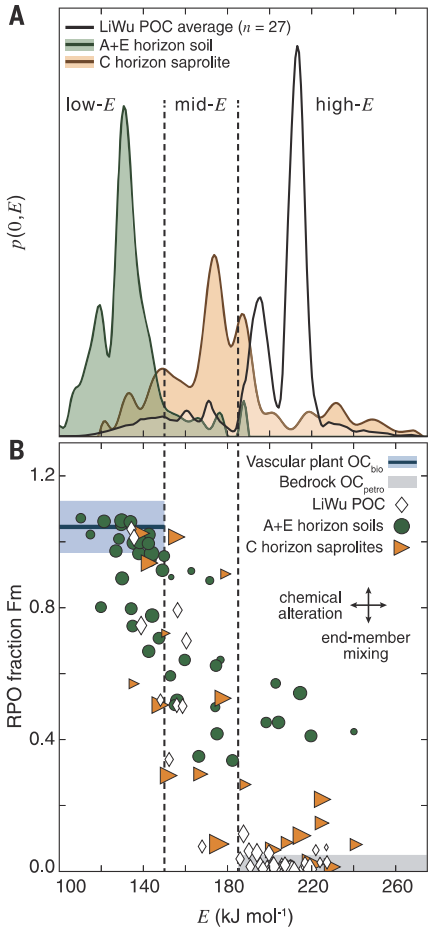

Fig. 2. Evidence for OC_{petro} chemical alteration. (**A**) Representative $p(0,E)$ distributions highlighting the differences between OC end-members: LiWu POC exported during typhoon events (average, n = 27; black), organic-rich A- and E-horizon topsoil (green), and C-horizon saprolite (orange). Each $p(0,E)$ distribution integrates to unity (y-axis values not shown) (*14*, *23*). (**B**) E versus Fm relationships for all soils (green circles and orange triangles) and LiWu POC (white diamonds) in which RPO-fraction ^{14}C activity was measured. Marker sizes represent the relative amount of total OC contained in each RPO fraction. Constraints on end-member E and Fm ranges are described in the text (blue, vascular plant OC_{bio}; gray, OC_{petro}). Black arrows represent theoretical trends for end-member mixing (vertical) and chemical alteration (horizontal) (*23*) and indicate that alteration is necessary to explain the presence of mid-E OC. In both panels, dashed lines separate OC into low-E (<150 kJ mol^{-1}), mid-E (150 ≤ E < 185 kJ mol^{-1}), and high-E (≥185 kJ mol^{-1}) regions. Fm error bars (±1σ) are smaller than marker sizes.

Energy distributions and ^{14}C activity in soil and saprolite materials provide strong evidence for OC_{petro} chemical alteration during weathering. Up to 51% of OC contained in saprolites and deep A and E horizons lies between 150 and 185 kJ mol^{-1} (termed mid-E; table S4 and fig. S4, B and C)—higher than values corresponding to vascular plant OC (<150 kJ mol^{-1}) yet lower than those for bedrock OC (≥185 kJ mol^{-1}). This observation could result from either (i) increasing vascular plant OC E by stabilization during aging in soils (*24*) or (ii) decreasing residual OC_{petro} E during oxidative weathering (*20*, *21*). We assessed the relative importance of these mechanisms by using the ^{14}C activity of each RPO fraction (table S5). As shown in Fig. 2B, low-E Fm values cluster near those of plant-wax fatty acids, whereas high-E material approaches an Fm value of zero. Meanwhile, mid-E OC spans an Fm range from 0.083 ± 0.002 to 0.912 ± 0.008. We rule out the possibility that ^{14}C-depleted mid-E OC exclusively reflects OC_{bio} aging because (i) this would require a biospheric component that has aged up to 20,000 ^{14}C years, much longer than the centennial soil residence times in Taiwan (*14*), and (ii) plant-wax fatty acids were not detected in some saprolite samples (table S6). Thus, mid-E material must reflect a mixture of weathered OC_{petro} and moderately aged OC_{bio}.

We treat OC_{petro} that has been chemically altered during weathering as a distinct end-member described by Fm = 0.0 and a value of f_{mid}, the fraction of $p(0,E)$ contained within the mid-E range, which is greater than the highest observed saprolite value of 0.51 (*14*). Figure 3A shows that all hillslope samples, with the exception of one unweathered saprolite, are adequately explained by a mixture of OC_{bio} and chemically altered OC_{petro}. This end-member is also present in LiWu River POC collected during typhoon floods, as evidenced by the divergence from a vertical mixing line between OC_{petro} and OC_{bio} in Fig. 3A. Therefore, along with unweathered bedrock OC (*19*) sourced from deep incision and landsliding (*11*), our approach detected catchment-scale export of chemically altered OC_{petro} from Central Range hillslopes during typhoon flood events. Because calculated f_{mid} depends on our choice of mid-E range (here, 150 to 185 kJ mol^{-1}), it is possible that mixing

trends and end-member compositions are sensitive to changes in *E* boundary values. We tested this sensitivity by allowing these boundary values to vary by ±10 kJ mol^{-1} (*14*). Although quantitative differences exist (fig. S5), the resultant mixing trends are qualitatively robust, indicating that the importance of chemically altered OC_{petro} is insensitive to our choice of mid-*E* boundary values.

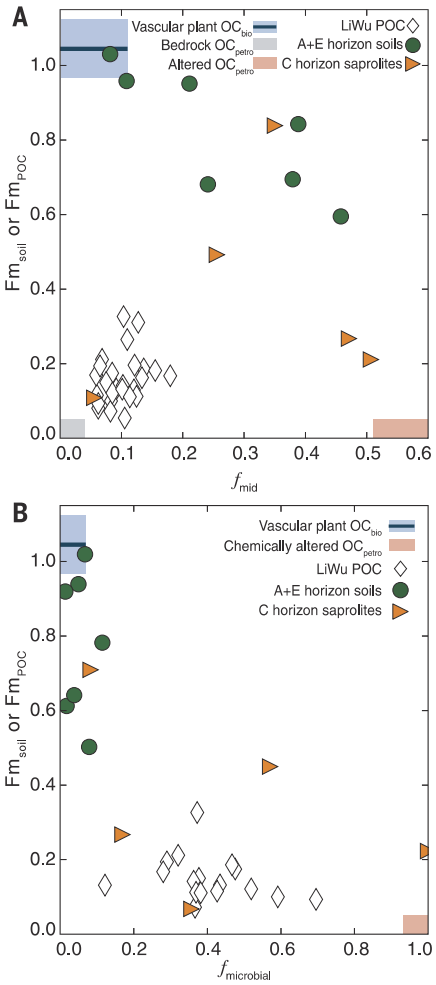

Fig. 3. Evidence for microbially mediated bedrock OC oxidation. (**A**) Bulk Fm versus f_{mid} relationships for soils (green circles and orange triangles) and LiWu POC (white diamonds). All soils, with the exception of the 0.5-m saprolite discussed in the text, are described by a mixing line between vascular plant OC_{bio} (blue) and chemically altered OC_{petro} (red) (*14*). LiWu River POC is dominated by bedrock OC_{petro} (gray) but does contain detectable chemically altered OC_{petro}, as evidenced by the deviation from a vertical mixing line between OC_{bio} and OC_{petro}. (**B**) Bulk Fm versus $f_{microbial}$ relationships for all samples in which fatty acid concentrations were analyzed (*14*). The relative abundance of microbial fatty acids increases with decreasing Fm across all samples, suggesting that microbial respiration is the source of chemically altered OC_{petro}. Measurement error bars (±1σ) are smaller than marker sizes.

Fatty acid molecular distributions and $\delta^{13}C$ values imply that rapidly oxidized OC_{petro} in soils is incorporated into microbial biomass, supporting laboratory-based incubation studies (*20*, *22*). We calculated $f_{microbial}$, the fraction of total fatty acids that are microbial in origin (*25*, *26*), as a proxy for the relative abundance of heterotrophic versus vascular plant biomass (*14*). This approach excludes fungal contributions and is thus a minimum estimate of heterotrophic biomass. Figure 3B shows that bulk Fm is negatively correlated with $f_{microbial}$ across all soil and POC samples. We do not expect this trend to be linear owing to fatty acid production biases (*25*, *26*). Still, this relationship suggests that heterotrophic biomass is more abundant in samples containing predominantly ^{14}C-free OC.

Sample limitation prevented measurement of microbial fatty acid ^{14}C activity (*14*), but the $\delta^{13}C$ values imply that bedrock OC is used as substrate (table S7) (*26*, *27*). Bulk OC and plant-wax fatty acid $\delta^{13}C$ values correlate strongly in A and E horizons (coefficient of determination $r^2 = 0.959$; $P < 0.001$; $n = 7$), reflecting the predominance of OC_{bio} in these samples, but are uncorrelated in C horizons ($P > 0.05$; $n = 4$) owing to a lack of OC_{bio} contribution to saprolites (fig. S6). Still, if OC_{bio} were the sole substrate for heterotrophs, then microbial and plant-wax fatty acid $\delta^{13}C$ values should correlate strongly with a constant $\delta^{13}C$ offset (*27*) in all samples. This is not apparent in either A- and E-horizon ($P > 0.05$; $n = 7$) or saprolite ($P > 0.05$; $n = 4$) samples, indicating that vascular plant OC cannot be the only substrate. Rather, this lack of correlation requires a secondary microbial carbon source (*20*–*22*), namely, bedrock OC. We conclude that mid-*E*, ^{14}C-free material is a product of microbial bedrock oxidation, produced either directly by extracellular enzymes or indirectly after acid hydrolysis (*20*), and is manifest as ^{14}C-depleted living biomass (*22*) or as residual, chemically altered OC_{petro} (*21*).

Substantial bedrock OC replacement in saprolites implies that considerable weathering occurs ≤1 m below the surface and that microbially mediated OC_{petro} oxidation can proceed at a pace matching the rapid exhumation in Taiwan. We propose that exhumation and hillslope erosion rates exert a first-order control on CO_2 emissions from OC_{petro} oxidation, because faster erosion will increase the rate of bedrock exposure to the weathering front (*8*). This is further supported by measurements of the dissolved rhenium flux from Taiwanese rivers, a proxy for OC_{petro} oxidation, which increases with erosion rate (*5*). However, the relationship between OC_{petro} oxidation and physical erosion rate cannot be linear. Large earthquakes and typhoons are known to cause widespread bedrock landsliding (*28*–*30*) and elevated export of OC_{petro} by rivers (*19*). Such events increase catchment-averaged erosion rates (*28*) but could decrease catchment-averaged OC_{petro} oxidation efficiency by bypassing the hillslope soil weathering window. OC_{petro} remineralization in Taiwan is incomplete, as evidenced by the abundance of bedrock OC in sediments exported by rivers (*19*) and deposited in nearby coastal margins (*31*). We predict a dampened response of OC_{petro}-derived CO_2 emissions to further increases in erosion rates, because increasing landslide rates will result in less catchment area available for soil formation and weathering.

Microbially mediated oxidative weathering in Taiwanese hillslope soils offsets geologic CO_2 drawdown and O_2 production by silicate weathering and OC_{bio} burial (*1*, *5*, *8*, *22*). The Φ_{ox} values calculated here are similar in magnitude to CO_2 source estimates from sulfide oxidation (≥22.9 ± 1.0 metric tons C km^{-2} year^{-1}; LiWu basin only) (*9*) and to CO_2 sinks from silicate weathering (3.1 ± 0.1 metric tons C km^{-2} year^{-1}; LiWu basin only; fig. S3C) (*18*) and OC_{bio} burial (21 ± 10 metric tons C km^{-2} year^{-1}; Taiwan average; fig. S3D) (*14*, *32*). This process is likely globally important, given that rapid soil formation is observed in other tropical and temperate orogenic settings such as the Southern Alps of New Zealand (*33*). We therefore hypothesize that CO_2 consumption is not favored in highly erosive mountain belts dominated by OC- and sulfide-rich low- and intermediate-grade metasedimentary lithologies. This comes from the observation that OC_{petro} and sulfide mineral oxidation is not limited by reaction kinetics even at high erosion rates (*5*, *8*, *21*), unlike silicate weathering and OC_{bio} export (*4*, *34*). Conversely, the magnitude of the net CO_2 sink likely increases with physical erosion rate in orogens dominated by high-grade metamorphic and igneous rocks owing to their lower OC_{petro} and sulfide contents. Although the global fluxes and the time scales over which they impact atmospheric CO_2 and O_2 concentrations remain to be assessed, our results demonstrate the importance of microbially mediated OC_{petro} oxidation and its relationship to tectonic and erosive controls on the global carbon cycle and Earth's long-term climate.

REFERENCES AND NOTES

1. N. M. Bergman, T. M. Lenton, A. J. Watson, **Am. J. Sci. 304**, 397–437 (2004).
2. P. Molnar, P. England, **Nature 346**, 29–34 (1990).
3. J. Gaillardet, B. Dupré, P. Louvat, C. J. Allègre, **Chem. Geol. 159**, 3–30 (1999).
4. V. Galy, B. Peucker-Ehrenbrink, T. Eglinton, **Nature 521**, 204–207 (2015).
5. R. G. Hilton, J. Gaillardet, D. Calmels, J.-L. Birck, **Earth Planet. Sci. Lett. 403**, 27–36 (2014).
6. M. A. Torres **et al.**, **Earth Planet. Sci. Lett. 450**, 381–391 (2016).
7. R. A. Berner, K. Caldeira, **Geology 25**, 955–956 (1997).
8. E. W. Bolton, R. A. Berner, S. T. Petsch, **Am. J. Sci. 306**, 575–615 (2006).
9. M. A. Torres, A. J. West, G. Li, **Nature 507**, 346–349 (2014).
10. S. J. Dadson **et al.**, **Nature 426**, 648–651 (2003).
11. N. Hovius, C. P. Stark, C. Hao-Tsu, L. Jiun-Chuan, **J. Geol. 108**, 73–89 (2000).
12. R. Emberson, N. Hovius, A. Galy, O. Marc, **Earth Surf. Dyn. 4**, 727–742 (2016).
13. K. Maher, C. P. Chamberlain, **Science 343**, 1502–1504 (2014).
14. Materials and methods are available as supplementary materials.
15. C.-C. Tsai, Z.-S. Chen, C.-T. Duh, F.-W. Horng, **Proc. Natl. Sci. Counc. Repub. China B 25**, 34–39 (2001).
16. O. Beyssac **et al.**, **Tectonics 26**, TC6001 (2007).
17. R. G. Hilton, A. Galy, N. Hovius, M.-J. Horng, H. Chen, **Geochim. Cosmochim. Acta 74**, 3164–3181 (2010).
18. D. Calmels **et al.**, **Earth Planet. Sci. Lett. 303**, 48–58 (2011).
19. R. G. Hilton, A. Galy, N. Hovius, M.-J. Horng, H. Chen, **Geology 39**, 71–74 (2011).

20. S. Schillawski, S. Petsch, Global Biogeochem. Cycles 22, GB3002 (2008).
21. S. Chang, R. A. Berner, Geochim. Cosmochim. Acta 63, 3301–3310 (1999).
22. S. T. Petsch, T. I. Eglington, K. J. Edwards, Science 292, 1127–1131 (2001).
23. J. D. Hemingway, D. H. Rothman, S. Z. Rosengard, V. V. Galy, Biogeosciences 14, 5099–5114 (2017).
24. R. G. Keil, L. M. Mayer, in Treatise on Geochemistry, H. Holland, K. Turekian, Eds. (Elsevier, 2014), vol. 12, chap. 12.
25. A. Frostegård, E. Bååth, Biol. Fertil. Soils 22, 59–65 (1996).
26. F. M. Hopkins et al., Soil Biol. Biochem. 76, 57–69 (2014).
27. N. Blair et al., Appl. Environ. Microbiol. 50, 996–1001 (1985).
28. N. Hovius et al., Earth Planet. Sci. Lett. 304, 347–355 (2011).
29. G. Li et al., Earth Planet. Sci. Lett. 472, 253–265 (2017).
30. O. Marc, N. Hovius, P. Meunier, T. Uchida, T. Gorum, J. Geophys. Res. Earth Surf. 121, 640–663 (2016).
31. L.-W. Zheng et al., Earth Planet. Sci. Lett. 465, 103–111 (2017).
32. R. G. Hilton et al., Global Biogeochem. Cycles 26, GB3014 (2012).
33. I. J. Larsen et al., Science 343, 637–640 (2014).
34. A. J. West, Geology 40, 811–814 (2012).

ACKNOWLEDGMENTS

We thank the NOSAMS (National Ocean Sciences Accelerator Mass Spectrometry) staff, especially M. Lardie-Gaylord and A. McNichol, and C. Johnson for laboratory assistance. J. Scheingross provided valuable comments on early versions of this manuscript. **Funding**: This research was supported by NSF Graduate Research Fellowship number 2012126152 and the WHOI Ocean Ventures Fund (J.D.H.); European Research Council Starting Grant 678779 ROC-CO2 (R.G.H.); and NSF grants OCE-0851015 and OCE-0928582 and WHOI Independent Study Award 27005306 (V.V.G.). **Author contributions**: J.D.H. and V.V.G. conceived the study; R.G.H., N.Ho., T.I.E., and M.-C.C. contributed samples and analytical tools; J.D.H., N.Ha., and L.W. performed laboratory measurements; J.D.H., R.G.H., N.Ha., L.W., and V.V.G. analyzed data; and J.D.H., R.G.H., N.Ho., and V.V.G. wrote the manuscript with input from all authors. **Competing interests**: None declared. **Data and materials availability**: All data are available in the supplementary materials.

SUPPLEMENTARY MATERIALS

www.sciencemag.org/content/360/6385/209/suppl/DC1
Materials and Methods
Supplementary Text
Figs. S1 to S6
Tables S1 to S8
References (35–65)

11 August 2017; accepted 21 February 2018
10.1126/science.aao6463

Science

Microbial oxidation of lithospheric organic carbon in rapidly eroding tropical mountain soils

Jordon D. Hemingway, Robert G. Hilton, Niels Hovius, Timothy I. Eglinton, Negar Haghipour, Lukas Wacker, Meng-Chiang Chen and Valier V. Galy

Science **360** (6385), 209-212.
DOI: 10.1126/science.aao6463

Microbes eat rocks and leave carbon dioxide

The reaction of atmospheric carbon dioxide (CO_2) with silicate rocks provides a carbon sink that helps counterbalance the release of CO_2 by volcanic degassing. However, some types of rocks contain petrogenic organic carbon, the oxidation of which adds CO_2 to the atmosphere, counteracting the drawdown by silicates. Hemingway *et al.* present evidence from the rapidly eroding Central Range of Taiwan showing that microbes oxidize roughly two-thirds of the petrogenic organic carbon there and that the rate of oxidation increases with the rate of erosion.

Science, this issue p. 209